JOURNAL OF PROPULSION AND POWER
Vol. 21, No. 4, July–August 2005

Kinematic Coupling Effects on Heat-Release Transfer Function of a Premixed Flame

H. Santosh* and R. I. Sujith†
Indian Institute of Technology, Chennai 600 036, India

The effect of acoustic excitation on the heat-release characteristics of a two-dimensional premixed flame is studied. Past researchers have assumed that the acoustic nearfield and kinematics of the flame surface are uncoupled. However, recent studies by the authors have shown that the acoustic nearfield is significantly affected by flame-surface wrinkling and hence the coupling between flame-surface kinematics and the acoustic field cannot be neglected. The acoustic-velocity nearfield of the flame surface is determined by using a boundary integral equation (BIE) modified to include the effects of flame-front wrinkling on the acoustic field. A linearized *G* equation is solved to obtain an expression for the flame-surface wrinkling in terms of the acoustic velocity at the flame front. This equation is then solved simultaneously with the BIE by using a Newton–Raphson scheme to obtain simultaneously the flame-surface shape and the acoustic-velocity variation for the case of a two-dimensional dump-stabilized flame. The results show that the transfer function is controlled by two parameters, the flame Strouhal number and the half-angle at the apex of the flame, θ. The computed transfer function is compared with the transfer functions from two other models. The first model assumes a one-dimesional variation of acoustic velocity along the axial direction. The second model assumes a two-dimensional acoustic-velocity field while neglecting kinematic coupling. The inclusion of kinematic coupling leads to the prediction of a different value of the magnitude of the transfer function at low frequencies. This difference in predicted magnitudes depends on the excitation velocity amplitude. The predicted magnitudes increase with decrease in θ. The predicted phase is observed to be insensitive to changes in θ. Kinematic coupling also results in the reduction of the predicted spatial variation of the magnitude of the normalized acoustic velocity along the flame.

Nomenclature

G	=	scalar field
$\mathcal{G}$	=	free-space Green's function
L_{flame}	=	length of flame from base to apex
p	=	acoustic pressure
q'	=	heat-release fluctuation
R	=	half-width of inlet
S_L	=	laminar flame speed
Sr	=	Strouhal number $= \omega R/s_L \cos\theta$
$u_{\bar{n}}$	=	acoustic velocity along local mean surface normal
X_f	=	flame-surface position along x axis
$\bar{X}_f$	=	mean surface position
ζ	=	flame-surface perturbation from the mean surface, along the mean surface normal
Θ	=	phase
θ	=	half the angle at the flame apex
ρ	=	mean density of gas
Φ	=	transfer function
ω	=	excitation frequency

Subscripts and Superscripts

*	=	nondimensional quantity
1D	=	one-dimensional model
d	=	value on the downstream side
$\bar{n}$	=	quantity along the local normal to the mean surface
$\hat{p}$	=	complex pressure amplitude
u	=	value on the upstream side
$\hat{u}_{\bar{n}}$	=	complex acoustic velocity amplitude
v	=	velocity

Received 12 March 2004; revision received 28 July 2004; accepted for publication 20 October 2004.

*Undergraduate Student, Department of Aerospace Engineering. Student Member AIAA.

†Associate Professor, Department of Aerospace Engineering; sujith@iitm.ac.in. Member AIAA.

I. Introduction

COMPLEX COMBUSTOR GEOMETRIES feature a large number of resonant acoustic modes. Acoustic waves traveling in such systems potentially affect and are affected by the combustion process driving in the system. These effects may take the form of fluctuations in heat release, which, depending on their relative phasing with the pressure oscillation, result in exchange of energy with the acoustic field. This energy exchange might then lead to noise, excessive vibration, instability, or even flame extinction, which can be detrimental to system health and performance.[1,2] To develop lower-order models for describing the thermoacoustic behavior of combustors, it is necessary to provide the transfer function between the heat release and the acoustic field.

Several attempts have been made to develop models of laminar premixed flames to predict the heat-release acoustic modulation transfer function. Merk[3] proposed a first-order model that predicted general trends of flame behavior. His analysis developed an analogy with electrical circuits to study the onset of instability in premixed burner-stabilized flames. Blackshear[4] has shown that flames behave very much like low-pass filters. Matsui[5] analyzed the amplification of acoustic waves by flames. His apparatus consisted of a premixed flame stabilized on a flat burner with different port arrangements. The flame was subjected to acoustic excitation from the upstream and pressure amplification was measured. The results were compared with several theoretical models, and a new model similar to Merk's was proposed.

McIntosh[6] studied the linearized response of the mass-burning rate of a premixed flame to rapid changes in pressure. The effect of pressure changes on a timescale of the order of the inverse of the square of nondimensional activation energy relative to the diffusion timescale were considered. This so-called "fast" timescale causes the reaction zone to take on a fundamentally different behavior governed by an unsteady diffusion-reaction equation. The response of the mass-burning rate to harmonic and four types of nonharmonic inputs were studied.

Boyer and Quinard[7] developed a linear kinematic model that was used to study the shape and dynamics of an anchored premixed flame. The dynamic response of the flame was modeled by introducing a relaxation-time parameter. The solution they obtained was identified with the analogous result in diffraction theory called the interference integral. Experimental results in which the flame shapes under different excitation modes were obtained by laser tomography were reported and compared with the theoretically predicted mode shapes.

Fleifel et al.[8] developed a one-dimensional kinematic model for an axis-symmetric premixed flame stabilized in a tube on an underlying Poiseuille mean flow profile, subjected to one-dimensional acoustic excitation. The heat-release oscillations were modeled as being caused by fluctuations in the burning area of the flame. Expressions for the interaction index n and time delay τ in the n–τ formalism were identified from the model developed.

DuCruix et al.[9] developed a model similar to that of Fleifel et al.[8] They compared the results obtained with experimental measurements of heat-release transfer functions for a conical premixed flame subjected to acoustic excitation. Good agreement between predicted and observed transfer-function magnitude and phase was reported for low excitation frequencies. Ferguson et al.[10] reported measurements of flame-surface-area oscillations. They showed that surface-area oscillations predict the magnitude of heat-release oscillations accurately but not the phase. Rook and de Goey[11] studied the response of burner-stabilized flat flames to acoustic perturbations. Two-dimensional transport equations for low-Mach-number reacting flows using a simple reaction mechanism were studied numerically. The influence of finite width perforations on the acoustic response of a flat flame was studied assuming a perfectly cooled burner. The characteristics of the transfer function for the burning-velocity fluctuations were studied.

Recently, Schuller et al.[12] have developed a unified model for the prediction of flame-transfer functions for the conical- and V-flame configurations. Transfer functions for different variations of modulating velocity have been derived. The dependence of the transfer function on Sr and θ was reported. The obtained results were compared with the transfer function obtained from numerical simulations of the G equation and experiment. It was shown that the model incorporating convective effects provided an improved prediction for the gain and the phase upon comparison with numerical simulations and experiments. The V flame was shown to behave like an amplifier over a certain range of frequencies.

Lee and Lieuwen[13] extended the model of Fleifel et al.[8] to include the effects of multidimensionality of the acoustic velocity at the flame front caused by the sudden change in gas properties. They examined the case of a dump-stabilized conical flame subjected to axial acoustic excitation. The local acoustic field was obtained from a boundary integral equation (BIE) derived by using a set of simplifying assumptions. This equation did not include the effect of flame-surface wrinkling on the acoustic field, caused by the variation of acoustic velocity along the flame surface. Rather, the flame-surface perturbation and hence the unsteady heat release were calculated using the computed acoustic velocity along the flame surface as a leading order input.

In all the preceding analyses, the oscillations in heat release are assumed to be caused by an increase in flame-surface area. This increase in area is caused by the wrinkling of the flame surface by acoustic velocity perturbations. Thus, the prediction of oscillations in heat release is dependent on the prediction of the acoustic-velocity variation along the flame surface. Previous analyses have assumed that the acoustic velocity nearfield of the flame is not affected by the wrinkling of the flame surface. Recent studies conducted by the authors[14] have shown that the effect of flame-surface wrinkling on the local acoustic field is considerable. This is true even when the length scale of wrinkling is small when compared to the acoustic wavelength but large when compared to the thickness of the reaction zone. Ferguson et al.[15] conducted particle image velocimetry measurements of the acoustic-velocity nearfield of a premixed conical flame in an axis-symmetric Rijke tube combustor and reported that the acoustic-velocity field shows considerable two-dimensional characteristics. Thus, the coupling between the acoustic-velocity field and the flame-surface kinematics cannot be neglected. Hence, the objective of this paper is to develop a model that includes the effect of this coupling in predicting the acoustic-velocity variation along the flame surface.

The rest of this paper is organized as follows: Section III describes the investigated geometry and provides details of the formulation and simplifying assumptions. Section IV derives an expression for calculating the heat-release acoustic-excitation transfer function. Section V gives details of the numerical formulation. The details of the cases examined and the nature of the results obtained are then discussed in Section VI. The paper closes with a qualitative comparison of the observed results with the experimental results of DuCruix et al.[9]

II. Analysis

The kinematic model of the flame described in this section is derived from Lee and Lieuwen.[13] Their formulation neglected the effect of coupling between flame-surface wrinkling and the local acoustic-velocity field. This work makes use of a modified integral equation derived in Santosh and Sujith[14] that includes this effect. The equations governing the acoustic field and flame-surface kinematics are obtained under the following assumptions:

1) The flame thickness is small compared to the wavelength of the modulating acoustic oscillation.

2) The reaction zone is compact. The flow upstream and downstream of the flame is isentropic.

3) The reaction chemistry is insensitive to pressure perturbations. Further, the laminar-burning velocity is assumed to be insensitive to flame-front wrinkling and is taken as a constant along the flame surface at all times.

4) The velocity perturbations are small when compared to the mean flow and hence the flame stays attached to the lip of the expansion at all times.

5) The mean flow velocity at the flame is one dimensional.

6) The mean flow Mach number of the fresh reactants $M \ll 1$. Consequently, all effects of $O(M)$ and higher are neglected.

The modified boundary integral equation is derived in the following subsection.

A. The Integral Equation

The general domain considered for the sake of the analysis presented in this subsection is shown in Fig. 1. The domain comprises an upstream region and a downstream region coupled at the flame surface. From the assumptions presented previously, the spatial variation of the acoustic-pressure field upstream and downstream of the flame surface is governed by the Helmholtz equation,

$$(\nabla^2 + k^2)p = 0 \tag{1}$$

Equation 1 can be transformed into a boundary integral equation by using the free-space Green's function $\mathcal{G}$.[16] This equation, called the Helmholtz integral equation, is presented here:

$$c(\boldsymbol{r})\,p(\boldsymbol{r}) = \int_{\bar{S}_1} \left[p(\boldsymbol{r}')\frac{\partial \mathcal{G}}{\partial \bar{n}} - \mathcal{G}\frac{\partial p}{\partial \bar{n}} \right] ds' \tag{2}$$

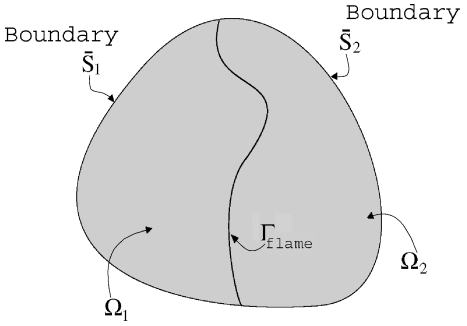

Fig. 1 General problem domain.

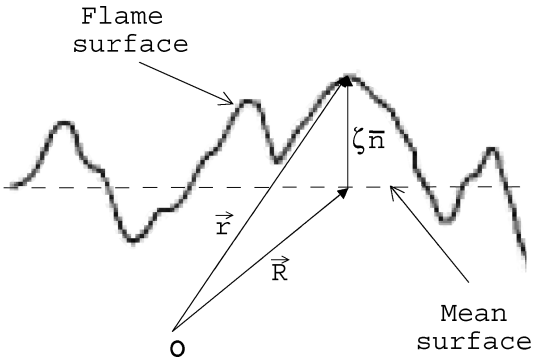

Fig. 2 Schematic of flame-surface geometry.

The domain of integration in Eq. (2) is the boundary of the upstream region and the mean flame surface. Equation (2) can be equivalently written for the downstream region also. However, for the purposes of analysis, the integral over the upstream region is considered.

In general, because the flame surface is moving, the acoustic pressure is given by the more general Ffowcs Williams–Hawkings integral equation. However, in this case, as will be presented in the next subsection, the amplitude of the flame-surface motions is assumed to be small. The mean flow Mach number is also very small. Thus, the Ffowcs Williams–Hawkings equation reduces to Helmholtz's integral equation in the frequency domain.

The coefficient of p on the left-hand side (LHS) of Eq. 2 is defined:

$$c(\boldsymbol{r}) = \begin{cases} 1 & \text{if} \quad \boldsymbol{r} \in \bar{\Omega} \\ \dfrac{1}{2} & \text{if} \quad \boldsymbol{r} \in \bar{S} \text{ and } \bar{S} \text{ is smooth at } \boldsymbol{r} \\ \dfrac{\alpha}{2\pi} & \text{if} \quad \boldsymbol{r} \in \bar{S} \text{ and } \bar{S} \text{ is nonsmooth at } \boldsymbol{r} \\ 0 & \text{otherwise} \end{cases} \tag{3}$$

where α is the included angle at the nonsmooth boundary point.[16]

The wrinkled flame surface can be represented as a perturbation from a mean surface as shown schematically in Fig. 2. The position vector of any point on the wrinkled flame surface can be represented as

$$\boldsymbol{r} = \boldsymbol{R} + \zeta \bar{n} \tag{4}$$

where ζ is the distance of the wrinkled flame surface from the mean surface as a function of arc length along the wrinkled flame surface. The vector $\bar{\boldsymbol{n}}$ is the local unit normal vector to the mean surface.

The acoustic pressure at the wrinkled flame surface can be represented as a Taylor series expansion in terms of ζ around the acoustic pressure at the corresponding mean surface point as

$$p(\boldsymbol{r}) = \tilde{p}(\boldsymbol{R}) + \zeta \frac{\partial \tilde{p}}{\partial \bar{n}} + \frac{\zeta^2}{2} \frac{\partial^2 \tilde{p}}{\partial \bar{n}^2} + \cdots \tag{5}$$

In this analysis, the wrinkling perturbations are assumed to be small. Thus, only terms up to $O(\zeta)$ in Eq. (5) are retained. Thus, the acoustic pressure at the wrinkled flame surface can be written as

$$p(\boldsymbol{r}) = \tilde{p}(\boldsymbol{R}) + \zeta \frac{\partial \tilde{p}}{\partial \bar{n}} \tag{6}$$

where the $(\sim)$ represents the value of the quantity at the mean surface.

The momentum equation in terms of acoustic quantities in the frequency domain is given by

$$-i\rho\omega \boldsymbol{u} = \boldsymbol{\nabla} p \tag{7}$$

Substituting for p in Eq. (7) from Eq. (6) and resolving along $\bar{n}$ on both sides, the following equation can be obtained for the acoustic velocity at the wrinkled surface along $\bar{n}$:

$$-i\omega\rho u_{\bar{n}} = \frac{\partial \tilde{p}}{\partial \bar{n}} + \zeta \frac{\partial^2 \tilde{p}}{\partial \bar{n}^2} + \frac{\partial \zeta}{\partial \bar{n}} \frac{\partial \tilde{p}}{\partial \bar{n}} \tag{8}$$

The derivative of pressure in the second term of Eq. (8) is $O(k^2 \tilde{p})$ from Eq. (1). Dividing Eq. (8) by $i\omega\rho$, the second term is $O(k\zeta)$. Imposing the condition $k\zeta \ll 1$ and dropping the second term yields the following equation for the velocity at the flame surface in terms of the velocity at the mean surface:

$$u_{\bar{n}} = \tilde{u}_{\bar{n}} \left(1 + \frac{\partial \zeta}{\partial \bar{n}} \right) \tag{9}$$

The assumption $k\zeta \ll 1$ has been used in past analyses of acoustic scattering from rough surfaces under the Born approximation.[17,18] When Eqs. (6) and (9) are used in Eq. (2), they yield, after some algebra, the following equation for the acoustic pressure field:

$$c(\boldsymbol{r})\hat{p}(\boldsymbol{r}) = \int_{\bar{S}} \left[\hat{p}(\boldsymbol{r}') \frac{\partial \mathcal{G}}{\partial \bar{n}} + i\omega\rho \hat{u}_{\bar{n}} \mathcal{G} \right] ds' + \int_{\bar{\Gamma}_{\text{flame}}} i\omega\rho \hat{u}_{\bar{n}} \times \left[\left(\frac{\zeta}{1 + \partial\zeta/\partial\bar{n}} \right) \frac{\partial \mathcal{G}}{\partial \bar{n}} - \left(\frac{\partial\zeta/\partial\bar{n}}{1 + \partial\zeta/\partial\bar{n}} \right) \mathcal{G} \right] ds' \tag{10}$$

The second integral is due to the presence of flame wrinkling alone. The following section derives a model for the kinematics of the flame surface.

B. Kinematic Model

The details of the investigated geometry are presented schematically in Fig. 3. The entire geometry including the flame surface is assumed to be two dimensional. The details of the flame-surface geometry are illustrated in Fig. 4. The flame surface can be described by a scalar function $G(\boldsymbol{r}, t) = 0$. A point on this surface moves with a velocity given by $\boldsymbol{V}_{\text{flame}} = \boldsymbol{v} - s_L \boldsymbol{n}$ where $\boldsymbol{v}$ is the velocity of the fresh mixture and $\boldsymbol{n} = \boldsymbol{\nabla} G / |\boldsymbol{\nabla} G|$ is the local normal to the flame front, pointing into the burnt gases. Along the flame surface, $(\mathrm{d}G/\mathrm{d}t)_{\text{flame}} = (\partial/\partial t + \boldsymbol{V}_{\text{flame}} \cdot \boldsymbol{\nabla}) G = 0$, which yields the following (Markstein[19]):

$$\frac{\partial G}{\partial t} + \boldsymbol{v} \cdot \boldsymbol{\nabla} G = s_L |\boldsymbol{\nabla} G| \tag{11}$$

Equation (11) is referred to in the combustion literature as the G equation. This equation is written in the ξ-η coordinate system (see Fig. 4). This choice of coordinate system was used in the analyses of Boyer and Quinard[7] and Schuller et al.[12] Setting $G(\boldsymbol{r}, t) = \xi - \zeta(\eta, t)$, where $\zeta(\eta, t)$ gives the location of the flame surface along the ξ axis, Eq. (11) becomes

$$\frac{\partial \zeta}{\partial t} + u_\eta \frac{\partial \zeta}{\partial \eta} = u_\xi - s_L \sqrt{1 + \left(\frac{\partial \zeta}{\partial \eta} \right)^2} \tag{12}$$

where u_ξ and u_η are the velocities along the ξ and η directions, respectively. The perturbation of the flame surface from the mean surface ζ and flame surface slope $\partial\zeta/\partial\eta$ are assumed to be small. The velocities u_ξ and u_η can be decomposed into mean and fluctuating parts as $u_\xi = \bar{U}_\xi + u'_\xi$, $u_\eta = \bar{U}_\eta + u'_\eta$. These expressions are substituted in Eq. (12) and only terms that are first order in the fluctuating variables, flame-surface slope, and perturbation are retained. As a result of this operation and assumption 5, Eq. (12) becomes

$$\frac{\partial \zeta}{\partial t} + \bar{U}_\eta \frac{\partial \zeta}{\partial \eta} = \bar{U}_\xi - s_L + u'_\xi \tag{13}$$

Equation 13 can be further decomposed into two equations for mean and fluctuating components to yield the following:

$$\bar{U}_\xi - s_L = 0 \tag{14}$$

$$\frac{\partial \zeta}{\partial t} + \bar{U}_\eta \frac{\partial \zeta}{\partial \eta} = u'_\xi \tag{15}$$

where u'_ξ is seen to be the acoustic velocity along the direction normal to the mean surface $u_{\bar{n}}$. Henceforth, $u_{\bar{n}}$ is used throughout.

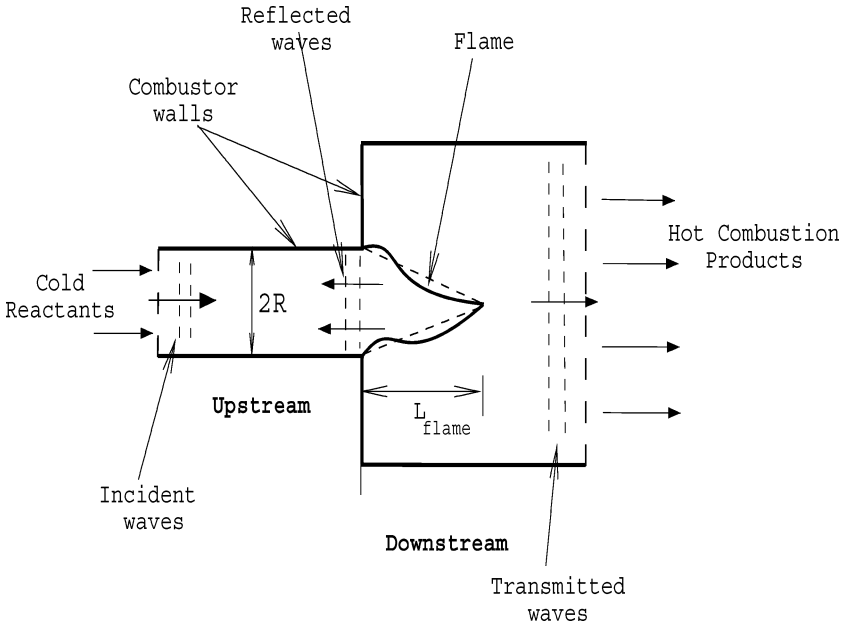

Fig. 3 Schematic of investigated geometry.

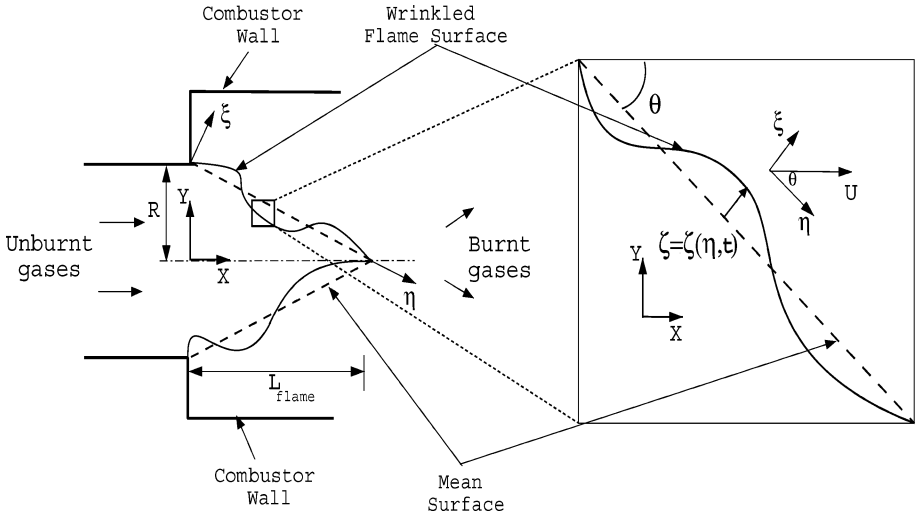

Fig. 4 Schematic of flame-surface geometry.

In the analysis that follows, the following nondimensionalization scheme is adopted. $\zeta^* = \zeta/R$, $y^* = y/R$, $\eta^* = \eta/R$, and $u'^*_{\bar{n}} = u'_{\bar{n}}/(s_L \cos\theta)$. The flame-surface perturbation is assumed to be harmonic. Therefore, all time-varying quantities can be written as $a'(\eta, t) = \hat{a}(\eta)e^{i\omega t}$. Further, defining $\bar{y}^* = 1 - y^*$ and making the above transformations, Eq. (15) reduces to

$$\frac{d\zeta^*}{d\bar{y}^*} + iS_r\hat{\zeta}^* = \hat{u}^*_{\bar{n}} \tag{16}$$

where $\bar{y}^* = \eta \sin\theta$ (see Fig. 4). Equation (16) is a first-order linear ordinary differential equation in $\hat{\zeta}^*$. In accordance with assumption 4, the end condition $\hat{\zeta}^*(0) = 0$ is applied. Further, because the boundary condition is symmetric, the solution is symmetric about the axis of symmetry of the mean surface. Thus, for the upper half of the flame surface, the solution to Eq. (16) is given by

$$\hat{\zeta}^*(\bar{y}^*) = \int_0^{\bar{y}^*} \hat{u}^*_{\bar{n}}(l^*)e^{-iS_r(\bar{y}^* - l^*)}dl^* \tag{17}$$

The solution presented in Eq. (17) is used in Eq. (10) to determine the acoustic-velocity field at the flame surface. The ζ in Eq. (10) is the instantaneous value of flame-surface perturbation. This is given by the real part of Eq. (17) ($= \mathrm{Re}[R\hat{\zeta}^* e^{i\omega t}]$). The combustor walls are assumed to be rigid. The flame is excited from upstream by specifying a constant input excitation velocity u_{exc} along the upstream inlet. The nonreflecting boundary condition ($Z = \rho c$) is applied at the downstream exit. This is to ensure that any acoustic-wave incident on the exit just travels out of the exit without reflections. Practically, this may be realized by choosing a very long exit-duct length. In realistic situations, however, more complicated boundary conditions apply. However, the wavefields resulting from these conditions can be constructed by using the canonical boundary conditions stated previously.

The boundary conditions at the flame are not known a priori. Therefore, matching conditions relating the acoustic pressure and velocity on the upstream and downstream sides of the flame are used. These matching conditions have been derived several times in the past.[20,21] The acoustic pressure and velocity jump across the flame are seen to be $O(M^2)$ and $O(M)$ respectively. Therefore, to the accuracy of the analysis considered in this paper (assumption 6),

these matching conditions reduce to

$$\hat{p}'_{\mathrm{u}} - \hat{p}'_{\mathrm{d}} = 0 \tag{18}$$

$$(\hat{u}'_{\bar{n}})_{\mathrm{u}} - (\hat{u}'_{\bar{n}})_{\mathrm{d}} = 0 \tag{19}$$

These matching conditions are applied in terms of the value of pressure and normal acoustic velocity at the wrinkled surface. Thus, the location of application of these conditions is amplitude dependent. Thus, substitution of the real part of Eq. (17) into Eq. (10) yields an integral equation that is nonlinear in $\hat{u}_{\bar{n}}$.

III. Transfer Function

The transfer function relates the oscillation in the heat release to the applied acoustic excitation. These oscillations in heat release are due to the variation in flame-surface area caused by wrinkling. This wrinkling is caused as a result of perturbations in the flame surface area resulting from modulation of local flow velocity by acoustic oscillations. The wrinkling causes a net increase in burning area, thereby causing the heat release to oscillate. In general, these oscillations are affected by the spatial variation of burning velocity resulting from flame-front curvature and stretch caused by increase in the burning area.[22,23] Following DuCruix et al.,[9] these effects are neglected in this work. Neglecting these effects, however, will serve to ascertain the importance of spatial variation of burning velocity in the prediction of the transfer function.

In all the discussion that follows, the flame surface shown schematically in Fig. 4 is assumed to have unit width. Therefore, the rate of heat release at the flame is given by

$$q = \int_{S_{\mathrm{flame}}} \rho_u s_L \Delta h dS \tag{20}$$

where Δh is the heat of reaction per unit mass for the mixture. Decomposing the variation in surface area S and heat release q into mean and fluctuating parts and retaining only linear terms in the perturbation yields

$$\bar{Q} + q' = \int_{\bar{S}_{\mathrm{flame}}} \rho_u s_L \Delta h d\bar{S} + \int_{\bar{S}_{\mathrm{flame}}} \rho_u s_L \Delta h dS' \tag{21}$$

The first of the two terms on the right-hand side (RHS) can be identified as the mean heat-release rate $\bar{Q}$. The second arises because of the increase in the flame-surface area caused by flame-front wrinkling. Therefore, dividing Eq. (21) by $\bar{Q}$ yields, after a little algebra,

$$q'/\bar{Q} = S'/\bar{S} \tag{22}$$

From Fig. 4, the surface-area perturbation S' can be written to the first order in terms of $\hat{\zeta}^*$ as

$$S' = 2\beta R \int_0^1 \frac{d\hat{\zeta}^*}{dy^*} dy^* \tag{23}$$

where $\beta = \cot\theta$, θ being the angle of the mean surface with the combustor axis. The transfer function is defined as $\Phi = (q'/\bar{Q})/(\hat{u}_{\mathrm{ref}}/\bar{U})$, where $\hat{u}_{\mathrm{ref}}$ is a reference velocity. Because the velocity field in this analysis is spatially varying, $\hat{u}_{\mathrm{ref}}$ is chosen, following the procedure adopted in the experiments of DuCruix et al.,[9] to be the axial component of the acoustic velocity at the origin of coordinates. This velocity is obtained by differentiating Eq. (10) in the axial direction and evaluating the acoustic velocity at $\boldsymbol{r} = 0$, using the momentum equation.

Using Eq. (23) in Eq. (22) yields, upon simplification, an expression for the transfer function as

$$\Phi(Sr, \beta) = \frac{2\bar{U}\beta R}{\hat{u}_{\mathrm{ref}}\bar{S}} \int_0^1 \hat{u}^*_{\bar{n}}(l^*) e^{-iS_r l^*} dl^* \tag{24}$$

Clearly the transfer function is seen to be a function of the flame Strouhal number and the half-angle θ at the apex of the flame. From Eq. (14) this angle is seen to be given by the quantity $\bar{U}/s_L$. Also, it can be observed that the transfer function is a correlation between a quantity $u^*_{\bar{n}}$ that varies over an acoustic wavelength and $e^{is_r l^*}$ that varies over a convective length. The next section details the specific cases that were investigated.

IV. Numerical Formulation

The entire computational domain was divided into upstream and downstream regions that are coupled at the flame front. The boundary of each region is discretized into linear elements. The acoustic pressure p and acoustic velocity $u_{\bar{n}}$ along each element are approximated by constant shape functions. The final discretized form of Eq. 10 is presented next.[14]

$$\frac{1}{2}\hat{p}_i = \sum_{j=1}^{j=N} (\hat{p}_j b_{ij} + i\omega\rho\hat{u}_{\bar{n}j} a_{ij}) + \sum_{j=n_f}^{j=N_f} i\omega\rho\hat{u}_{\bar{n}j}(\tilde{\psi}_{ij} + \tilde{\psi}'_{ij}) \tag{25}$$

The coefficients a_{ij} and b_{ij} and the flame pertubation functions $\tilde{\psi}$ and $\tilde{\psi}'$ in two dimensions are given by

$$a_{ij} = \frac{i}{4}\int_{\Gamma_j} H_0^1(k|\boldsymbol{r}_i - \boldsymbol{r}'_j|)ds'$$

$$b_{ij} = \frac{-ik}{4}\int_{\Gamma_j} H_1^1(k|\boldsymbol{r}_i - \boldsymbol{r}'_j|)\frac{[(\boldsymbol{r}_i - \boldsymbol{r}'_j)\cdot\bar{n}_j]}{|\boldsymbol{r}_i - \boldsymbol{r}'_j|}ds'$$

$$\tilde{\psi}'_{ij} = \frac{i}{4}\int_{\Gamma_j}\left(\frac{\partial\zeta/\partial\bar{n}(\boldsymbol{r})}{1+\partial\zeta/\partial\bar{n}}\right)H_0^1(k|\boldsymbol{r}_i - \boldsymbol{r}'_j|)ds'$$

$$\tilde{\psi}_{ij} = \frac{-ik}{4}\int_{\Gamma_j}\left(\frac{\zeta(\boldsymbol{r})}{1+\partial\zeta/\partial\bar{n}}\right)H_1^1(k|\boldsymbol{r}_i - \boldsymbol{r}'_j|)\frac{[(\boldsymbol{r}_i - \boldsymbol{r}'_j)\cdot\bar{n}_j]}{|\boldsymbol{r}_i - \boldsymbol{r}'_j|}ds'$$

where H_1^0 and H_1^1 are the Hankel's functions of the first and second kind respectively. The free-space Green's function of the Helmholtz equation is given by the Hankel's function. The singular integral a_{ii} was evaluated exactly. The result is presented next[24]:

$$a_{ii} = \Delta\{1 + (2i/\pi)[\log(k\Delta/4) + \gamma_e - 1]\} + O(k\Delta^2) \tag{26}$$

where Δ is the length of the ith element. The singular part of integral $\tilde{\psi}'_{ii}$ is evaluated using a logarithmic quadrature scheme.

Comparison with the analytical result for a straight transverse temperature jump in a straight duct without using the kinematic model gave errors in acoustic pressure of magnitude less than 1% for $k\Delta < 0.1$, where k is the excitation wavenumber on the side of the unburnt reactants. This was checked for various positions of the temperature jump in the duct. All integrals were evaluated using a 20-point Gauss quadrature. The acoustic field was also obtained for the geometry of interest neglecting the kinematics of the flame surface. These results were found to agree with those of Lieuwen.[25]

V. Results and Discussion

In all the cases investigated, the ratio of inlet to exit diameters was fixed at 0.5 and the radius of the inlet was fixed at $R = 0.025$ m. Results were obtained for the value of burning velocity, $s_L = 0.2\ \mathrm{ms}^{-1}$, and three values of mean flow velocity ($\bar{U}/s_L = 2.21$, 2.98, and 4.12). The upstream and downstream excitation velocity amplitude were maintained at $0.1\ \mathrm{ms}^{-1}$. The temperatures of the fresh mixture (T_{u}) and burnt gases (T_{b}) were fixed at 300 K and 1000 K respectively. The results obtained are compared with two other models. The first of these is the transfer function obtained assuming a constant one-dimensional variation of acoustic velocity at the flame (DuCruix et al.[9]). Assuming $\hat{u}^*_{\bar{n}} = \hat{u}_{\mathrm{ref}}/s_L\beta$ in Eq. (24), the following expressions for the magnitude and phase of the one-dimensional transfer function are obtained:

$$|\Phi^{1\mathrm{D}}(Sr)| = \frac{\sqrt{2(1-\cos Sr)}}{Sr} \tag{27}$$

$$\Theta^{1D}(Sr) = \tan^{-1}\left(\frac{1-\cos Sr}{\sin Sr}\right) \tag{28}$$

This model will be referred to as the one-dimensional model in all the discussion that follows.

The second model is derived from that of Lee and Lieuwen.[13] In this model, the acoustic field is assumed to be unaffected by the wrinkling of the flame front. Thus the second integral in Eq. (10) is neglected and what remains is just the Helmholtz integral equation. This equation is solved for the same boundary conditions and matching conditions [Eqs. (18) and (19)]. The acoustic velocity along the flame obtained from this solution is used in Eq. (24) to obtain the transfer function. This will be referred to as the quasi-kinematic model (QKM) model in all the discussion that follows. The present model shall be referred to as the linear kinematic model (LKM).

Figure 5 illustrates a typical result and plots the instantaneous acoustic pressure isobars and velocity vectors nearfield of the flame. The acoustic velocity field shows strong two-dimensional characteristics. This strong two-dimensionality arises as a result of flame-surface wrinkling.

Figure 6 plots the variation of the magnitude and phase of the transfer function for the three values of $\bar{U}/s_L$ as a function of

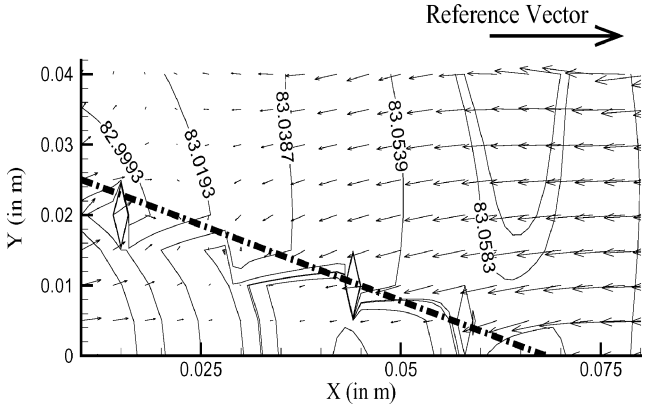

Fig. 5 Computed instantaneous acoustic-pressure isobars and velocity vectors. $s_L = 0.2$ ms^{-1}, $R = 0.025$ m, $T_b/T_u = 3.33$, $\omega t = 0$, $Sr = 62.53$ (75 Hz), reference vector = 0.05 ms^{-1}. The flame is excited from downstream. The thick broken line shows the position of the mean surface.

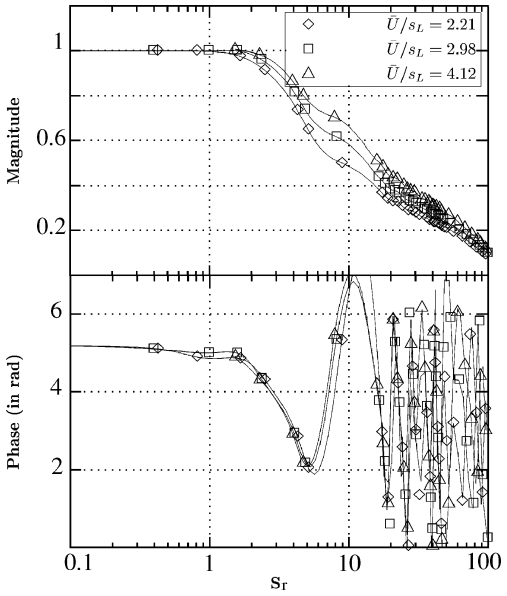

Fig. 6 Variation of the magnitude (top) and phase (bottom) of the transfer function with Strouhal number as predicted by the LKM model. The flame is excited from upstream; $s_L = 0.2$ ms^{-1}, $R = 0.025$ m, and $T_b/T_u = 3.33$.

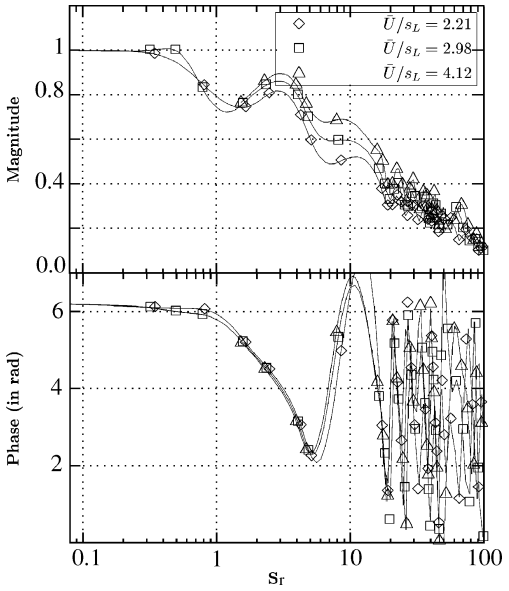

Fig. 7 Variation of the magnitude (top) and phase (bottom) of the transfer function with Strouhal number as predicted by the LKM model. The flame is excited from downstream; $s_L = 0.2$ ms^{-1}, $R = 0.025$ m, and $T_b/T_u = 3.33$.

Strouhal number for the flame being excited from upstream. The magnitude of the transfer function is seen to decrease and finally become nearly zero at high Strouhal numbers. Figure 7 plots the variation of the magnitude and phase of the transfer function for the flame being excited from the downstream end. The magnitude of the transfer function decreases with increasing Strouhal number. Thus the flame behaves like a lowpass filter. At high Strouhal numbers the difference between the convective lengthscale R and the acoustic lengthscale is large. Thus the correlation between $\hat{u}_n^*$ (varying over an acoustic wavelength) and the oscillatory term (varying over a convective length) in Eq. (24) is poor. Therefore, the magnitude of the transfer function decreases at high Strouhal numbers. The magnitude of the transfer function is seen to increase with an increase in $\bar{U}/s_L$ under both excitation cases as can be seen from Figs. 6 and 7.

The phase of the transfer function plotted in Fig. 6 and Fig. 7, for the cases of upstream and downstream excitation respectively, is seen to weakly depend on the variation of $\bar{U}/s_L$. This is because the spatial variation of the phase of the acoustic velocity along the flame in this analysis depends only on the excitation frequency and is insensitive to variations in $\bar{U}/s_L$.

Figure 8 plots the variation of the magnitude and phase of the transfer function ($\bar{U}/s_L = 2.98$) with Strouhal number, calculated using the three models, for the flame being excited from upstream. The QKM predicts the largest magnitude at low Strouhal numbers. The prediction from the LKM differs from the QKM at low Strouhal numbers. However, at Strouhal numbers greater than 8, the agreement is better. Figure 9 plots the variation of the magnitude and phase of the transfer function for the same case as above except that the excitation is from downstream. The LKM predicts a lower magnitude when compared to the QKM for Strouhal numbers less than 15 at this excitation velocity amplitude. At Strouhal numbers greater than 15, the prediction is seen to be higher than the QKM prediction in some cases. Furthermore, the LKM prediction shows a dependence on excitation velocity. These issues are discussed in the following paragraphs.

The transfer function in Eq. (24) can be seen to be a continuous superposition of flame-wrinkling waves. These waves interfere constructively or destructively depending on the correlation between the acoustic lengthscale and the lengthscale of the flame wrinkles. The effect of this interference is a net increase or decrease in burning area, which in the framework of the current analysis leads to an increase or decrease in the magnitude of the transfer function.

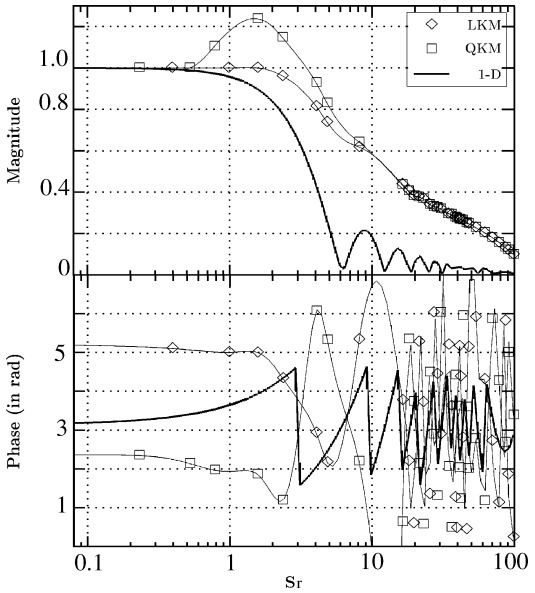

Fig. 8 Variation of the magnitude (top) and phase (bottom) of the transfer function with Strouhal number. The flame is excited from upstream; $\bar{U}/s_L = 2.98$, $R = 0.025$ m, and $T_b/T_u = 3.33$.

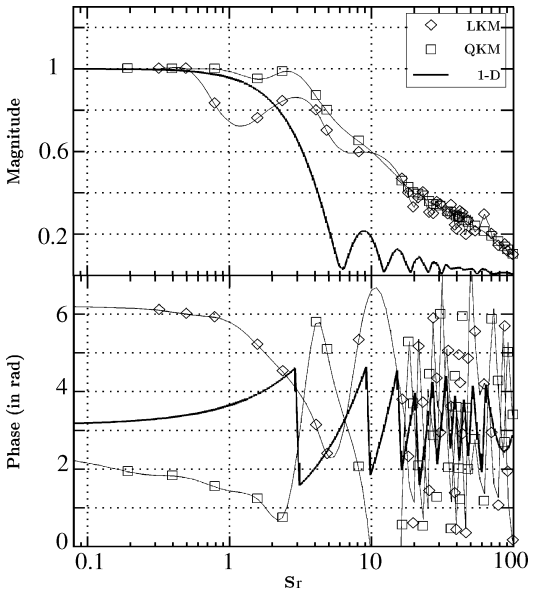

Fig. 9 Variation of the magnitude (top) and phase (bottom) of the transfer function with Strouhal number. The flame is excited from downstream; $\bar{U}/s_L = 2.98$, $R = 0.025$ m, and $T_b/T_u = 3.33$.

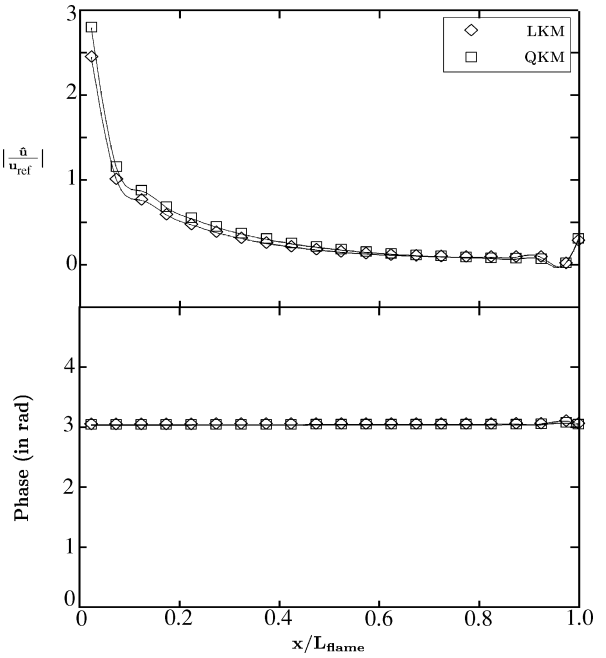

Fig. 10 Variation of the magnitude (top) and phase (bottom) of the acoustic velocity along the flame surface at $Sr = 4.0$; $\bar{U}/s_L = 2.98$, $R = 0.025$ m, and $T_b/T_u = 3.33$, upstream excitation.

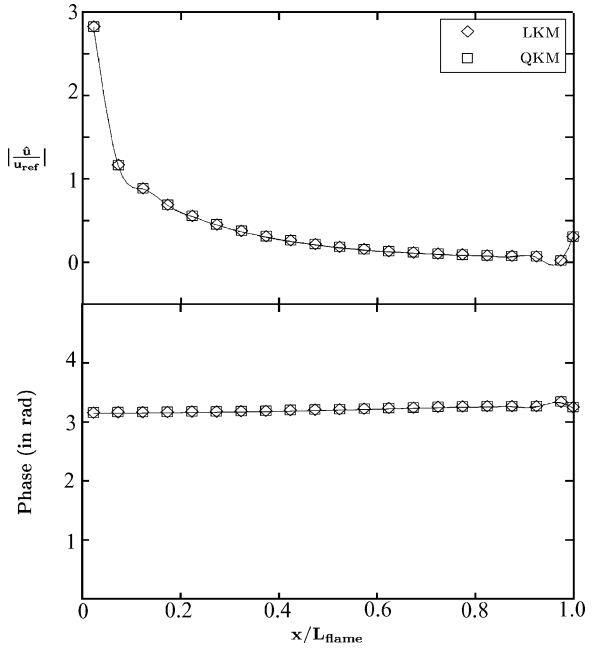

Fig. 11 Variation of the magnitude (top) and phase (bottom) of the acoustic velocity along the flame surface at $Sr = 100.0$; $\bar{U}/s_L = 2.98$, $R = 0.025$ m, and $T_b/T_u = 3.33$, upstream excitation.

Figures 10 and 11 plot a typical variation of magnitude and phase of the normalized acoustic velocity $\hat{u}'_{\bar{n}}/\hat{u}_{\text{ref}}$ along the flame as predicted by both models. The Strouhal numbers are 4.1 and 100.0, respectively, $\bar{U}/s_L = 2.98$, and the excitation is from the upstream side. The acoustic velocity magnitude is lesser in the case of the LKM for the case of $Sr = 4.1$. However, the case $Sr = 100.0$ shows no difference between the LKM and the QKM predictions. This difference in velocity distribution leads to the predicted transfer-function magnitude being lower in the case of LKM at low Strouhal numbers. Figures 12 and 13 plot the variation of acoustic velocity magnitude and phase along the flame surface for Strouhal numbers 4.1 and 100. The excitation is from the downstream side. The spatial variation of velocity magnitude predicted by the LKM model is seen to be more uniform than the variation predicted by the QKM for $Sr = 4.1$. Furthermore, the difference in the predicted phase is seen to be large at $Sr = 4.1$. This leads to the difference in the predicted transfer-function magnitude at low frequencies because of increased destructive interference as previously discussed. It was observed that the inclusion of kinematic-coupling resulted in the reduction of the normalized acoustic-velocity magnitude in all the cases investigated at this excitation amplitude. The agreement with the 1D model in all cases is seen to be poor except at Strouhal numbers close to 1.

The amplitude dependent nature of the matching conditions [Eqs. (18) and (19)] results in a nonlinear integral equation for the acoustic pressure and velocity field. Thus, it may be expected that the transfer function in either excitation case shows a dependence on the excitation-velocity amplitude. This was observed in the results. Figure 14 illustrates a typical result. The variation of

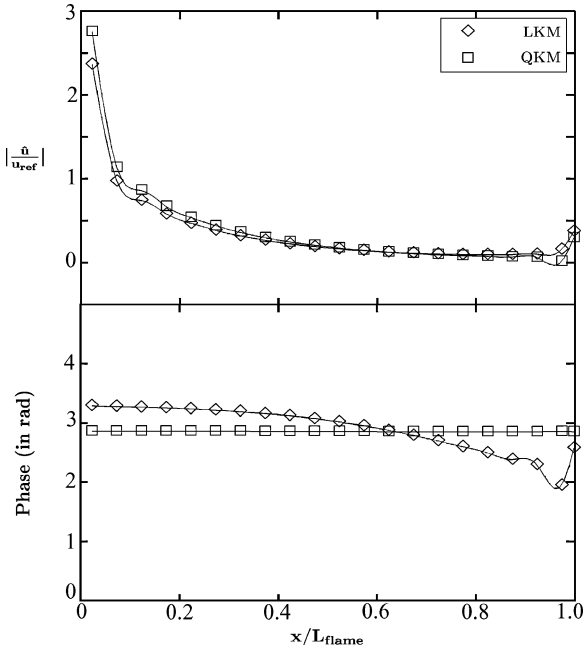

Fig. 12 Variation of the magnitude (top) and phase (bottom) of the acoustic velocity along the flame surface at $Sr = 4.0$; $\bar{U}/s_L = 2.98$, $R = 0.025$ m, and $T_b/T_u = 3.33$, downstream excitation.

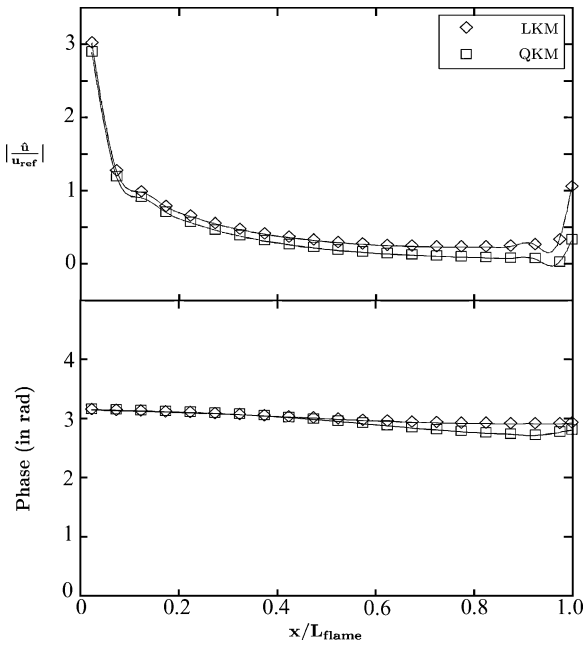

Fig. 13 Variation of the magnitude (top) and phase (bottom) of the acoustic velocity along the flame surface at $Sr = 100.0$; $\bar{U}/s_L = 2.98$, $R = 0.025$ m, and $T_b/T_u = 3.33$, downstream excitation.

transfer-function magnitude with excitation velocity as predicted by the LKM and the QKM is presented. The excitation Strouhal number is $Sr = 4.1$, and the flame is excited from the downstream end. The difference in the predictions increases with the increase in excitation velocities. This result may be explained by the increasingly strong constructive interference of flame-wrinkling waves as has been discussed previously. In other cases examined, the transfer-function magnitude reduces with increase in excitation velocity. Thus, it may be inferred that kinematic coupling modifies the nature of the interference of flame-wrinkling waves, leading to either an increase or decrease in the burning area. The magnitude in the case of the QKM was observed to be constant as may be expected over the same range of excitation.

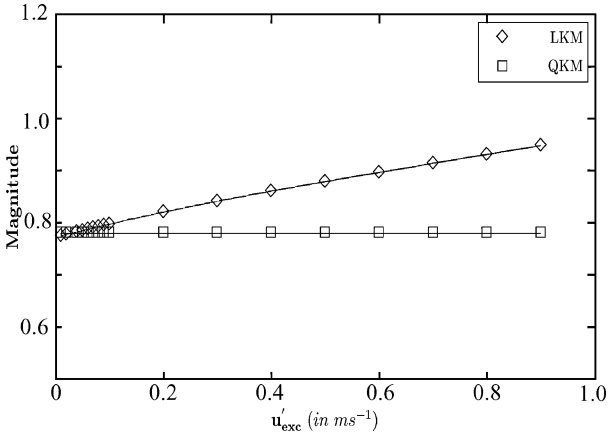

Fig. 14 Variation of the magnitude of the transfer function as a function of the excitation velocity; $Sr = 4.1$, $\bar{U}/s_L = 2.98$, $R = 0.025$ m, and $T_b/T_u = 3.33$, downstream excitation.

VI. Conclusions

This paper examines the effect of kinematic coupling on the prediction of the heat-release transfer function of a premixed flame. The results are compared with two other models. First, by assuming a one-dimensional axial acoustic excitation and second, by including the effect of multidimensionality of the acoustic field but neglecting kinematic coupling. The response of the flame was characterized under both upstream and downstream excitation.

The transfer function was seen to be a continuous superposition of waves that interfere constructively or destructively, resulting in an increase or decrease in the burning area of the flame, resulting in turn in a corresponding increase or decrease in the magnitude of the transfer function. The magnitude of the transfer function predicted by the QKM is different from that predicted by the LKM. The agreement with the 1D model was seen to be poor. The magnitude of the transfer function increases with increase in the value of $\bar{U}/s_L$. The phase of the transfer function is insensitive to changes in $\bar{U}/s_L$. This is because the phase of the transfer function depends only on the phase of the acoustic velocity along the flame, which in this analysis is independent of $\bar{U}$.

The prediction of the spatial variation of acoustic velocity is seen to be sensitive to the effect of flame wrinkling. It is observed that the presence of wrinkling leads to a reduction in the acoustic-velocity magnitude along the flame, especially under downstream excitation. This effect is not captured by the QKM. Further, the amplitude-dependent nature of the matching conditions used results in the dependence of the transfer function on the excitation velocity. It was observed that the magnitude of the transfer function either increases or decreases with increase in the excitation amplitude.

The present model is developed entirely in the frequency domain using a linearized form of the G equation [Eq. (13)]. This effectively neglects the interactions between the individual harmonic components of flame-surface wrinkling. Also, the present model does not consider variations in burning velocity along the flame caused by flame wrinkling. Thus, heat-release oscillation occurs purely because of increase in the burning area of the flame. Thus the prediction in the phase of the heat release is poor. Heat-release transfer-function measurements on conical flames of DuCruix et al.[9] show an increase in phase with excitation Strouhal number. The present models on the other hand predict an oscillatory variation of phase with Strouhal number. Thus, a more complete nonlinear model with a time-domain formulation that considers effects of burning-velocity variation resulting from flame-front curvature may be successful in predicting the phase of the heat-release oscillations.

References

[1]Putnam, A. A., and Dennis, W. R., "Organ Pipe Oscillations in a Flame-Filled Tube," *Proceedings of the Combustion Institute*, Vol. 4, 1953, pp. 566–575.

[2]Barrere, M., and Williams, F. A., "Comparison of Combustion Instabilities Found in Various Types of Combustion Chambers," *Proceedings of the Combustion Institute*, Vol. 12, 1968, pp. 169–181.

[3]Merk, H. J., "An Analysis of Unstable Combustion of Premixed Gases," *Proceedings of the Combustion Institute*, Vol. 6, 1956, pp. 500–512.

[4]Blackshear, P. L., "Driving Standing Waves by Heat Addition," *Proceedings of the Combustion Institute*, Vol. 4, 1953, pp. 533–566.

[5]Matsui, Y., "An Experimental Study on Pyro-Acoustic Amplification of Premixed Flames," *Combustion and Flame*, Vol. 43, 1981, pp. 199–209.

[6]McIntosh, A. C., "The Linearised Response of the Mass Burning Rate of a Premixed Flame To Rapid Pressure Changes," *Combustion Science and Technology*, Vol. 91, Nos. 4–6, 1993, pp. 329–346.

[7]Boyer, L., and Quinard, J., "On the Dynamics of Anchored Flames," *Combustion and Flame*, Vol. 82, No. 7, 1990, pp. 51–65.

[8]Fleifel, M., Annaswamy, A. M., Ghoneim, Z. A., and Ghoneim, A. F., "Response of a Laminar Premixed Flame to Flow Oscillations: A Kinematic Model and Thermoacoustic Instability Results," *Combustion and Flame*, Vol. 106, No. 4, 1996, pp. 487–510.

[9]DuCruix, S., Durox, D., and Candel, S., "Theoretical and Experimental Determinations of the Transfer Function of a Laminar Premixed Flame," *Proceedings of the Combustion Institute*, Vol. 28, 2000, pp. 765–773.

[10]Ferguson, D., Richards, G. A., Woodruff, S., Bernal, S., and Gautam, M., "Effect of Surface Area Variation on Heat Release Rates in Premixed Flames," *Proceedings of the Second Joint Meeting of the U.S. Sections of the Combustion Institute*, Combustion Inst., 2001.

[11]Rook, R., and de Goey, L. P. H.,"The Acoustic Response of Burner Stabilized Flat Flames: A Two-Dimensional Numerical Analysis," *Combustion and Flame*, Vol. 133, Nos. 1–2, 2002, pp. 119–132.

[12]Schuller, T., Durox, D., and Candel, S., "A Unified Model for the Prediction of Laminar Flame Transfer Functions: Comparisons Between Conical and V-Flame Dynamics," *Combustion and Flame*, Vol. 134, Nos. 1–2, 2003, pp. 21–34.

[13]Lee, D. H., and Lieuwen, T. C., "Premixed Flame Dynamics in a Longitudanal Acoustic Field," *Journal of Propulsion and Power*, Vol. 19, No. 5, 2003, pp. 837–846.

[14]Santosh, H., and Sujith, R. I., "Acoustic Near-Field Characteristics of a Wrinkled Premixed Flame," AIAA Paper 2003-5093, July 2003.

[15]Ferguson, D., Richards, G. A., and Woodruff, S., "Acoustic Velocity Measurements in a Naturally Oscillating Flame," *Proceedings of the Third Joint Meeting of the U.S. Sections of the Combustion Institute*, Combustion Inst., 2003.

[16]Chen, G., and Zhou, J., *Boundary Element Methods*, Academic Press, Burlington, MA, 1992.

[17]Thorsos, E., "The Validity of the Kirchoff Approximation for Rough Surface Scattering Using a Gaussian Roughness Spectrum," *Journal of the Acoustical Society of America*, Vol. 83, No. 1, 1988, pp. 79–92.

[18]Thorsos, E., "The Validity of the Perturbation Approximation for Rough Surface Scattering Using a Gaussian Roughness Spectrum," *Journal of the Acoustical Society of America*, Vol. 86, No. 1, 1989, pp. 261–277.

[19]Markstein, G. H., *Nonsteady Flame Propagation*, Pergamon, New York, 1964.

[20]McIntosh, A. C., "Pressure Disturbances of Different Length Scales Interacting with Conventional Flames," *Combustion Science and Technology*, Vol. 75, 1991, pp. 287–309.

[21]Lieuwen, T. C., "Theoretical Investigation of Unsteady Flow Interactions with a Premixed Planar Flame," *Journal of Fluid Mechanics*, Vol. 435, 2001, pp. 289–303.

[22]Matalon, M., "On Flame Stretch," *Combustion Science and Technology*, Vol. 31, 1983, pp. 169–181.

[23]Chung, S. H. and Law, C. K., "An Invariant Derivation for Flame Stretch," *Combustion and Flame*, Vol. 55, No. 1, 1984, pp. 123–125.

[24]Abramowitz, A., and Stegun, I., *Handbook of Mathematical Functions*, 9th ed., Dover, New York, 1972.

[25]Lieuwen, T. C., "Investigation of Combustion Instability Mechanisms in Premixed Gas Turbines," Ph.D. Dissertation, Aerospace Engineering Dept., Georgia Inst. of Technology, Atlanta, GA, Aug. 1998.